IEEE Access
Multidisciplinary | Rapid Review | Open Access Journal

Received October 9, 2019, accepted October 29, 2019, date of publication November 4, 2019, date of current version November 13, 2019.

Digital Object Identifier 10.1109/ACCESS.2019.2951059

Interference of Spread-Spectrum Modulated Disturbances on Digital Communication Channels

FRANCESCO MUSOLINO, (Member, IEEE), AND PAOLO S. CROVETTI, (Member, IEEE)
Department of Electronics and Telecommunications, Politecnico di Torino, 10129 Torino, Italy
Corresponding author: Paolo S. Crovetti (paolo.crovetti@polito.it)

ABSTRACT In this paper, the effects of random spread spectrum (SS) electromagnetic interference (EMI) on digital communications are addressed. For this purpose, the influence of EMI on a communication channel is described in the framework of information theory in terms of an equivalent channel capacity loss, which is analytically predicted and validated by experimental results. The EMI-induced channel capacity loss for non-modulated and SS-modulated interference generated by a switching-mode DC-DC power converter are then evaluated for different EMI and channel characteristics so that to compare different scenarios of practical interest.

INDEX TERMS Spread spectrum, electromagnetic compatibility (EMC), electromagnetic interference (EMI), DC-DC converters, digital communications, channel capacity.

I. INTRODUCTION

Electromagnetic interference (EMI) from switching-mode power converters and digital equipment can be easily coupled to susceptible communication blocks within the same module or integrated circuit, due to parasitic coupling through the power distribution network, through the package and/or through the silicon substrate and can be a threat to the operation of present-day information and communication technology (ICT) electronic systems inducing malfunctions ranging from the degradation of the bit error rate (BER) up to the complete failures [1]–[6]. As a consequence, EMI needs to be carefully controlled in the very first design stages at architectural and integrated circuit level to assure the proper operation of complex systems with no penalty in terms of costs, time-to-market and performance, and also in order to meet the more and more stringent Electromagnetic Compatibility (EMC) regulations [7]–[10].

In this context, several techniques have been devised to address EMI at circuit and architectural level [11]–[14]. In particular, the techniques based on the frequency modulation of critical switching signals, generally known as *Spread-Spectrum (SS) techniques*, have been extensively proposed as simple, low cost solutions to mitigate EMC problems and are widely employed in practice [13].

Spread-spectrum techniques have been introduced as a mean to reduce the peak value of EMI spectrum since the middle of 1990s with specific reference to switching power converters and digital clocked equipment [15], [16]. In these works, the influence of the modulation parameters on the harmonic peak values has been highlighted and some optimizations in terms of EMI performance have been made. More recently, advanced SS techniques like the random and chaotic modulations [17]–[19], which provide better spectral characteristics and a smoother energy spreading around the switching frequency, have been proposed. As far as the power converters are concerned, further investigations have also been aimed to determine the impact of SS modulations on the converter performance like efficiency, output ripple and input current distortion [20]–[25]. Based on the results of SS research, many SS oscillator IC topologies have been proposed in recent literature and have been commercialized as standalone clock generators and also embedded into microprocessor/microcontroller units and integrated power converters [26]–[29].

The effects of SS on the spectral characteristics of EMI have been extensively studied in the last years and a significant (10-20 dB) reduction of the peaks of EMI spectra measured following EMC standards [7]–[10] has been generally reported. While this reduction helps to comply with EMC regulations, which just take into account the peak of EMI spectra, the real value of SS techniques as a mean to reduce the potential adverse effects of EMI in practical applications is a more controversial matter and has been sometimes questioned [30]–[32].

In [30], in particular, SS modulated interference has shown to have worse effects on the signal quality of digital video and audio broadcasting than non-SS-modulated interference.

The associate editor coordinating the review of this manuscript and approving it for publication was Filbert Juwono.

At the same time, the effectiveness of SS techniques in mitigating interference in a case of practical importance has been shown in [33], where a digital circuit with SS clock has been considered as an aggressor and an analog FM radio as a victim. Moreover, a minimum impact of SS modulation on broadband digital TV has been reported in [31].

In such a scenario, a theoretical evidence of the effectiveness of SS modulation in reducing the interfering potential of switching signals has not been shown so far and, although the effectiveness of SS techniques is nowadays generally accepted, it has been experimentally observed just in very specific applications [33], and it is not yet fully clear what kind of benefit can be expected by electronic circuits and systems designers by adopting SS techniques in their products with the intent to preserve functionality of potentially interfering parts. In particular, the effectiveness of SS techniques in low-frequency switching-mode electronic power converters as a mean to avoid interference with baseband ICT digital systems has not been specifically addressed.

In this paper, aiming to provide circuit designers with some insight on the benefits and limits of SS techniques in general terms and without focusing just on EMC regulation requirements, the effect of random SS-modulated interference on communication channels is described in terms of equivalent channel capacity loss and compared with non-SS-modulated EMI. In this framework, the impact of EMI generated by a SS switching-mode power converter on a digital data line - in terms of channel capacity reduction and increased BER - is experimentally investigated.

The paper is organized as follows: in Section II, the spectral characteristics of EMI originating from non-SS and SS power converters and digital systems and their potential interference with ICT equipment is presented. Focusing on such a scenario, a description of the adverse effects of EMI on a communication channel in terms of capacity loss is introduced in Section III and validated in Section IV with reference to the results of experiments carried out on a DC-DC power converter electromagnetically coupled to a digital data line. The approach introduced in Section III is then adopted to study the impact of random SS modulations on channel capacity on a theoretical basis in Section V and is then contextualized in Section VI, where practical application cases are discussed. Finally in Section VII, some concluding remarks are drawn.

II. COMMUNICATION CHANNEL AND EMI MODELLING

The effects of non-modulated and SS-modulated EMI on a communication channel, as schematically depicted in Fig.1a, are focused in this paper. In this section, the hypotheses on the communication channel and on EMI considered through the paper are stated and the models employed in the following are introduced.

A. CHANNEL MODELLING

Communication over a band-limited linear channel, corrupted by additive white Gaussian noise (AWGN) with unilateral power spectral density N_0 is considered. The transmitted

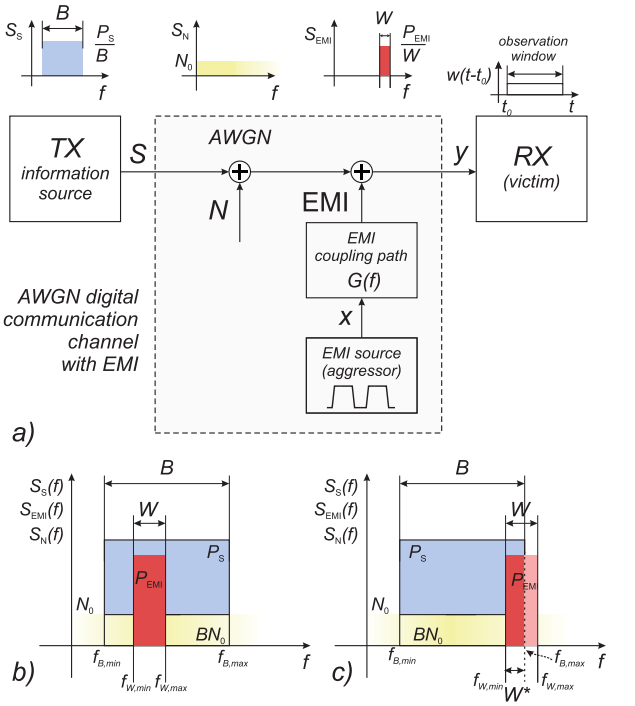

FIGURE 1. Model of a digital communication channel operating in the presence of EMI: a) block diagram, b) power spectral densities of the nominal received signal ($S_S(f)$), the background noise at the receiver ($S_N(f)$) and coupled EMI ($S_{EMI}(f)$), whose bandwidth W is fully included in the signal bandwidth B, c) as in b), where the EMI bandwidth W and the signal bandwidth B are partially overlapped ($W^\star = B \bigcap W$).

signal is described as a wide-sense stationary (WSS) gaussian random process independent of the channel noise process, with a total power P_S and a power spectral density (p.s.d.) P_S/B constant over the channel bandwidth[1] B, as depicted in Fig.1a. Under the above hypotheses, the channel capacity C_0, that gives the upper bound of the information than can be reliably transmitted over the channel in the unit time, is given by the Shannon-Hartley equation [34]:

$$C_0 = B \log_2 \left(1 + \frac{P_S}{BN_0}\right) = B \log_2 (1 + \alpha) \qquad (1)$$

where

$$\alpha = \frac{P_S}{BN_0}$$

is the signal-to-noise ratio (SNR) of the AWGN channel.

B. PERIODIC AND SS-MODULATED EMI MODELLING

In this framework, it is now assumed that the communication channel is also corrupted by narrowband EMI generated by an aggressor whose operation is based on periodic or randomly SS-modulated switching signals, like a switching-mode power converter or a digital circuit, and electromagnetically coupled with the nominal signal path via the transfer function $G(f)$, as illustrated in Fig.1a.

[1] In the following B will be used to indicate both the interval $(f_{B,min}, f_{B,max})$ and its extension, i.e. $|f_{B,max} - f_{B,min}|$, the meaning being clear from the context.

If the aggressor signal $x(t)$ originating interference (e.g. the clock signal in a digital circuit or the control signal of power transistors in a converter) is periodic with period $T = 1/f_0$, it can be represented in terms of its Fourier series expansion

$$x(t) = \sum_{x=-\infty}^{+\infty} c_k e^{j2\pi k f_0 t} \tag{2}$$

and the p.s.d. $S_{\mathrm{EMI}}(f)$ of EMI coupled with a victim equipment can be written as

$$S_{\mathrm{EMI}}(f) = \sum_{k=0}^{+\infty} |G(kf_0)|^2 |c_k|^2 \delta(f - kf_0) \tag{3}$$

in which $G(f)$ describes EMI coupling and $\delta(\cdot)$ is the Dirac distribution.

Aiming to the reduction of the EMI p.s.d. at harmonic frequencies kf_0, SS techniques consist in the application of a frequency modulation to periodic waveforms originating interference, which actually translate the original periodic interfering signal $x(t)$ in (2) into

$$x_{\mathrm{SS}}(t) = \sum_{k=-\infty}^{+\infty} c_k e^{j2\pi k f_0 \, t + j2\pi k \delta f_0 \int_{-\infty}^{t} \xi(\tau) \mathrm{d}\tau} \tag{4}$$

where f_0 is the central frequency, δ is the modulation depth and $0 \leq \xi(t) \leq 1$ is the modulation profile. If a piece-wise constant random modulation profile

$$\xi(t) = \sum_{k} r_k \Pi_T(t - kT) \tag{5}$$

is considered, where

$$\Pi_X(x) = \begin{cases} 1 & 0 < x < X \\ \frac{1}{2} & x = 0 \wedge x = X \\ 0 & \text{elsewhere,} \end{cases}$$

and $r_k \in [0, 1]$ is a random or chaos-based SS modulation, the EMI spectral power can be more or less uniformly spread over the bandwidth $[kf_0, kf_0(1 + \delta)]$. Under the hypothesis that $\xi(t)$ varies slowly compared with $1/\delta f_0$, in particular, it has been shown [13] that the p.s.d. $S_{\mathrm{EMI,SS}}(f)$ of EMI coupled with a victim equipment can be expressed as

$$S_{\mathrm{EMI,SS}}(f) = |G(f)|^2 \sum_{k=0}^{+\infty} |c_k|^2 \frac{1}{k\delta f_0} \cdot \rho\left(\frac{f - kf_0}{k\delta f_0}\right) \tag{6}$$

where $\rho(x)$ is the amplitude probability density (a.p.d.) function of the modulation profile $\xi(t)$. Since the a.p.d. $\rho(x)$ is normalized to one, the k-th harmonic EMI power content

$$P_{\mathrm{EMI},k} = \int_{kf_0}^{kf_0(1+\delta)} S_{\mathrm{EMI,SS}}(f) \mathrm{d}f = |G(kf_0)|^2 |c_k|^2$$

is the same as in (3), but being the same power spread over a wider bandwidth $k\delta f_0$, the peak value of the p.s.d. around the k-th harmonic frequency,

$$S_{\mathrm{EMI},k,\max} = \max_{f \in [kf_0, kf_0(1+\delta)]} S_{\mathrm{EMI,SS}}(f)$$

can be reduced down to $P_k/k\delta f_0$ if $\rho(x)$ is uniform in the [0, 1] interval. This condition, which is clearly the most desirable for EMC compliance will be specifically focused in what follows.

Even if (6) holds under the hypothesis of a slowly varying modulation profile $\xi(t)$ and has been considered above to obtain a simple approximate expression of the p.s.d. of SS signals, the analysis presented in what follows does not rely on the assumption of quasi-static variations of the modulation profile $\xi(t)$ in (6). In particular, a fast-varying modulation profile $\xi(t)$, which changes randomly on a period-by-period basis according to (5), in which random variables r_k are mutually uncorrelated, will be always considered in experiments.

More specifically, it will be assumed that the variations of the modulation profile $\xi(t)$ during the finite observation window $w(t)$ in which the receiver in Fig.1 acquires a data packet are fast enough so that

$$\begin{aligned} S_{\mathrm{EMI,SS},t_0}(f) &= \left| \int_{-\infty}^{\infty} x_{\mathrm{EMI,SS}}(\tau) w(\tau - t_0) e^{-j2\pi f \tau} \mathrm{d}\tau \right|^2 \\ &\simeq \mathbb{E}_{t_0}\left\{ S_{\mathrm{EMI,SS},t_0}(f) \right\} \simeq S_{\mathrm{EMI,SS}}(f) \quad \forall t_0, \end{aligned}$$

i.e. the short-term spectral characteristics of the EMI process during the observation window $w(t)$ do not depend on the initial observation time t_0 and can be conveniently approximated by the overall EMI p.s.d. $S_{\mathrm{EMI,SS}}(f)$. This guarantees that the variations of the modulation profile $\xi(t)$ in the observation window are relevant enough and lead to an effective short-term spreading of EMI spectral energy and to spectral peak reduction in standard EMC compliance tests, as detailed in [20].

C. MODELLING OF A COMMUNICATION CHANNEL AFFECTED BY EMI

Narrowband EMI around an harmonic frequency kf_0 superimposed onto the nominal signal in the bandwidth B of the communication channel in Fig.1a is modelled in what follows as a WSS narrowband random process with overall power P_{EMI} and bandwidth W, completely or partially overlapping the signal bandwidth B as shown in Fig.1b and 1c.

Moreover, it is assumed that the EMI process is statistically independent both of the channel noise, indicated as *background noise* hereafter, and of the transmitted signal. As a further hypothesis, an EMI process with a Gaussian a.p.d. is considered in what follows. This last assumption on the EMI a.p.d. is found to be in reasonable agreement with the statistics of measured EMI in practical cases, as discussed in [35] and confirmed by the time-domain waveforms and the a.p.d. of narrowband EMI shown in Fig.2, which refer to EMI generated by a Buck converter in a 50 kHz bandwidth around 100 kHz (left side, the circuit will be described in Section IV) and to a narrowband Gaussian random process (right side) with the same bandwidth and power. Moreover, a Gaussian amplitude distribution is the worst case a.p.d. in terms of interfering potential, as shown in [36], and it is

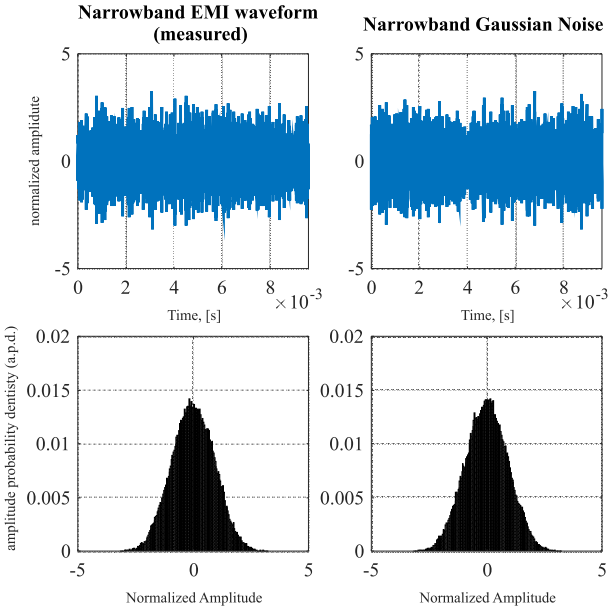

FIGURE 2. Time-domain waveforms and amplitude probability density (a.p.d.) of measured narrowband EMI generated by a DC-DC power converter (see Section IV for further details) in a 50 kHz bandwidth around 100 kHz (left) and narrowband Gaussian noise (white noise filtered over the same bandwidth of the EMI waveform).

therefore generally adopted in the field of communications to describe noise and interference.

III. EMI-INDUCED CHANNEL CAPACITY LOSS

In order to discuss the interfering potential of EMI on digital communications independently of specific hardware, modulations and protocols in different wired and wireless links, the effect of non-SS-modulated and random SS-modulated EMI on a generic communication channel is described in what follows in the framework of Shannon information theory as an equivalent EMI-induced channel capacity loss [34].

For this purpose, the capacity C of a communication channel in the presence of EMI, assuming that a single EMI harmonic overlaps completely or in part with the channel bandwith B as in Fig.1b or Fig.1c, can be calculated as

$$C = C_1 + C_2 \tag{7}$$

where C_1 is the capacity of sub-channel where the signal bandwidth overlaps with the EMI bandwidth, i.e. $W^\star = B \bigcap W$, and is given by

$$\begin{aligned} C_1 &= \int_{B\bigcap W} \log_2\left(1+\frac{S_S(f)}{S_N(f)+S_{EMI}(f)}\right) df \\ &= W^\star \log_2\left(1+\frac{P_S}{N_0\, B+\frac{B}{W}P_{EMI}}\right) \\ &= W^\star \log_2\left(1+\frac{\alpha}{1+\frac{B}{W}\alpha\beta}\right) \end{aligned} \tag{8}$$

where:

$$S_S(f) = \frac{P_S}{B}\Pi_B(f - f_{B,\min})$$

is the signal p.s.d.,

$$S_N(f) = N_0$$

is the background noise p.s.d.,

$$S_{EMI}(f) = \frac{P_{EMI}}{W}\Pi_W(f - f_{W,\min})$$

and is the EMI p.s.d. under the simplifying hypotheses considered above,

$$W^\star = \left[\max\left(f_{B_{\min}}, f_{W_{\min}}\right), \min\left(f_{B_{\max}}, f_{W_{\max}}\right)\right] \tag{9}$$

is the EMI overlap bandwidth and $\beta = P_{EMI}/P_S$ is the overall EMI-to-signal power ratio.

With the same notations, the capacity C_2 of the complementary sub-channel $B - B\bigcap W$, not affected by EMI, can be expressed as

$$\begin{aligned} C_2 &= \int_{B-B\bigcap W} \log_2\left(1+\frac{S_S(f)}{N_0}\right) df \\ &= \left(B - W^\star\right)\log_2\left(1+\alpha\right). \end{aligned} \tag{10}$$

Replacing (8) and (10) in (7), the overall channel capacity in the presence of EMI can be expressed in the form

$$\begin{aligned} C &= \left(B - W^\star\right)\log_2\left(1+\alpha\right) \\ &\quad + W^\star \log_2\left[\left(1+\alpha\right)\frac{1+\alpha+\frac{B}{W}\alpha\beta}{(1+\alpha)(1+\frac{B}{W}\alpha\beta)}\right] \\ &= C_0 + W^\star \log_2\left(1-\frac{\alpha}{1+\alpha}\frac{\alpha\beta}{\frac{W}{B}+\alpha\beta}\right) \\ &= C_0 + \Delta C\left(\alpha, \beta, W^\star, \frac{W}{B}\right) \end{aligned} \tag{11}$$

where C_0 is the capacity of the same channel without EMI as in (1) and ΔC is the channel capacity loss due to the presence of EMI.

$$\Delta C_k = \begin{cases} \Delta C\left[\alpha, \beta, \min\left(\delta k f_0, f_{B_{\max}} - k f_0\right), \dfrac{\delta k f_0}{B_2}\right] & \text{upspr.} \\ \Delta C\left[\alpha, \dfrac{\beta}{2}, \min\left(\dfrac{\delta k f_0}{2}, f_{B_{\max}} - k f_0\right), \dfrac{\delta k f_0}{B_1}\right] + \Delta C\left[\alpha, \dfrac{\beta}{2}, \min\left(\dfrac{\delta k f_0}{2}, k f_0 - f_{B_{\min}}\right), \dfrac{\delta k f_0}{B_2}\right] & \text{sym.} \\ \Delta C\left[\alpha, \beta, \min\left(\delta k f_0, k f_0 - f_{B_{\min}}\right), \dfrac{\delta k f_0}{B_1}\right] & \text{downspr.} \end{cases} \tag{12}$$

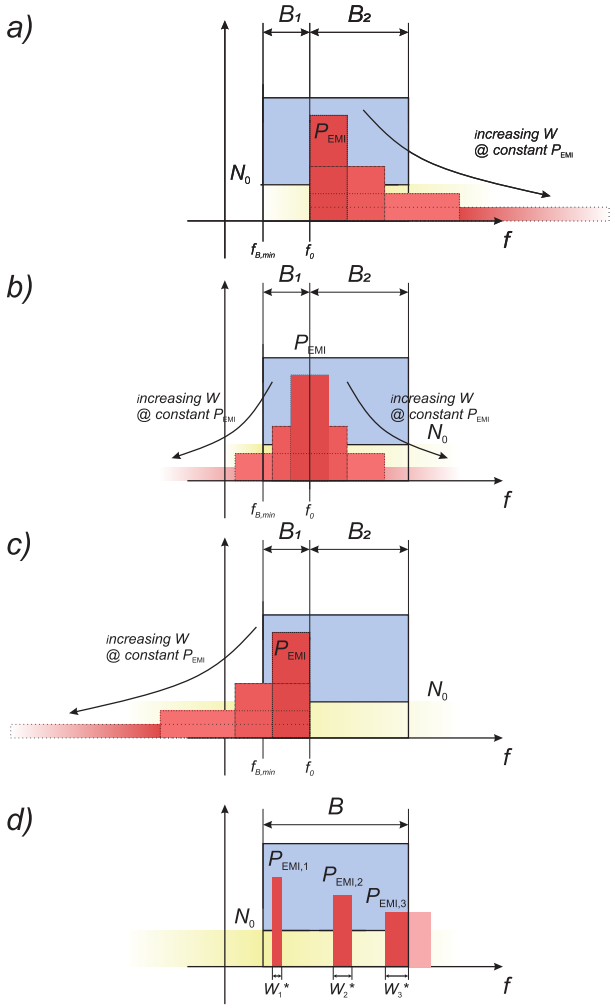

FIGURE 3. Nominal signal, background noise and EMI spectra considered in (12) and (13) for: a) up-spread SS modulation, with generic $f_0 \neq f_{B_{min}}$, b) symmetric SS modulation with central frequency f_0 c) down-spread SS modulation with generic upper frequency f_0, d) several EMI spectral lines in the signal bandwidth.

The analysis presented so far can be applied to calculate the capacity loss ΔC_k in an AWGN channel due to EMI at frequency kf_0 with up-spreading, symmetric and down-spreading SS modulations and modulation depth δ, by considering $W = \delta k f_0$ and appropriate values of $f_{W,\min}$ in (9) as outlined in Fig.3a-c, yielding the expression reported in (12), as shown at the bottom of the previous page.

Moreover, the analysis derived so far can be immediately extended to the case of more non-overlapping EMI spectral lines of Fig.3d, expressing the overall EMI-induced channel capacity loss ΔC_{TOT} by superposition of the capacity loss contributions due to each spectral line $k = N_1 \ldots N_2$ in the channel bandwidth.

$$\Delta C_{\mathrm{TOT}} = \sum_{k=N_1}^{N_2} \Delta C_k \tag{13}$$

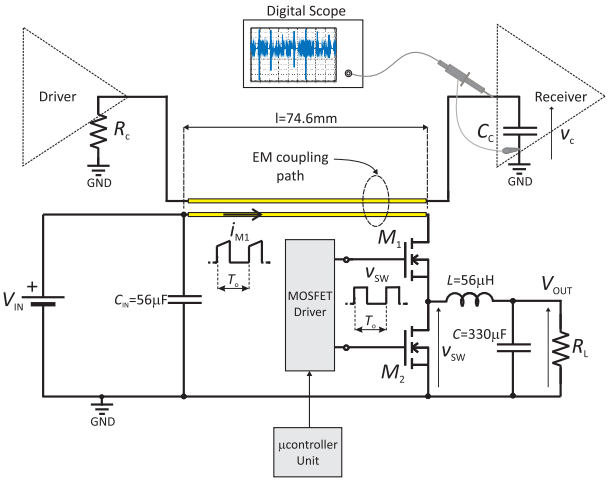

FIGURE 4. Schematic view of the test setup.

IV. VALIDATION

In this Section, the EMI-induced capacity loss model derived above is validated with reference to measured EMI. More specifically, the channel capacity predicted by (13) is compared to the channel capacity estimate obtained from the measured EMI p.s.d. on the basis of (1).

A. TEST SETUP

For validation purposes, the test setup in Fig.4, which is the same presented in [37], is considered. Here, a DC-DC power converter is intentionally designed to interfere with a digital data link. The converter is a hard-switched synchronous Buck operated from an input voltage $V_{\mathrm{IN}} = 16$ V and connected to a load $R_{\mathrm{L}} = 10\ \Omega$ in open-loop mode with a fixed duty cycle $D = 0.375$. Such a converter is driven by a 100 kHz PWM signal generated by a microcontroller. The data line is closed on $R_{\mathrm{c}} = 47\ \Omega$ and $C_{\mathrm{c}} = 100$ pF, which describe the output and the input impedances of the transmitter and of the receiver, respectively.

In order to couple the EMI from the power converter to the digital line, the converter has been designed on the specific two-layer test printed circuit board (PCB) shown in Fig.5a, where the power trace carrying the time varying current i_{M1} in Fig.4 and the data trace are routed close to each other, causing disturbances to propagate from the converter to the bus [37]. This test structure is considered here as a representative example of crosstalk due to inductive coupling, which can be easily found in practical applications and has been extensively discussed in EMC textbooks [38].

In particular, based on S-parameter measurements on the test PCB and taking into account of the line terminations in Fig.4, the transfer function between the current i_{M1} and the voltage v_{c} across the data receiver reveals a significant inductive coupling as observed in Fig.5b, which results in disturbances on the data line voltage v_{c} related to the time derivative of the current i_{M1}.

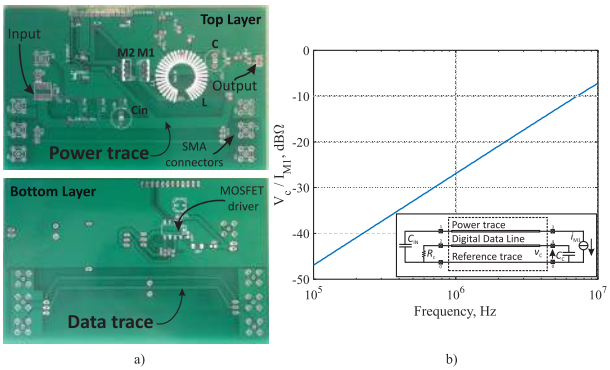

FIGURE 5. Test PCB: a) Top and bottom layers; b) transfer function between the current i_{M1} and the voltage v_c.

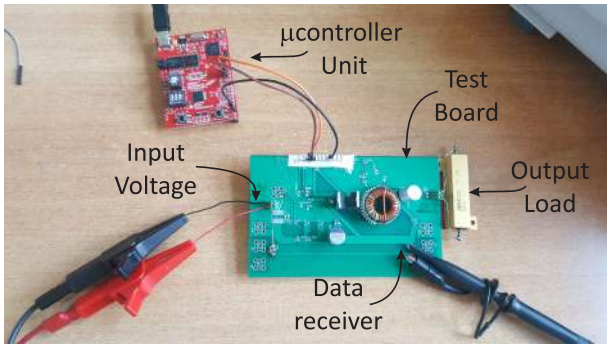

FIGURE 6. Picture of the test setup.

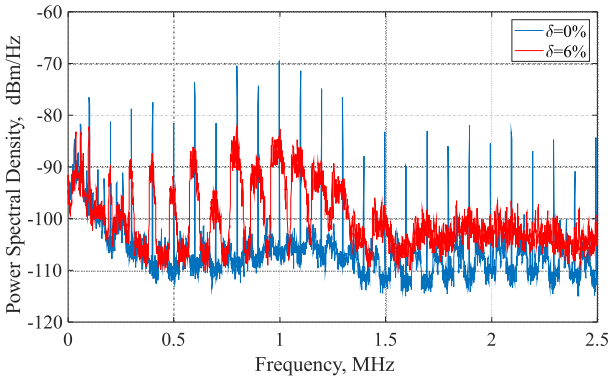

FIGURE 7. Power spectral density of periodic and random SS-modulated ($\delta = 6\%$) EMI coupled with the receiver in the 0-2.5 MHz bandwidth.

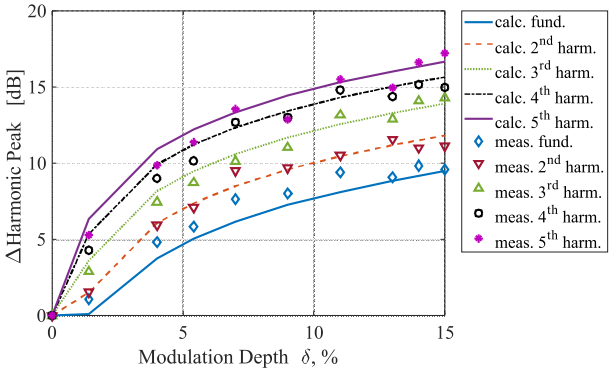

FIGURE 8. Difference between the peak amplitudes of the non modulated and random SS-modulated switching waveform V_{SW} at different modulation depth δ: measured results versus prediction.

The EMI voltage v_c at the receiver input is acquired with a digital scope at 125 MS/s during the DC-DC converter operation by the experimental setup in Fig.6. Its spectrum, which has been estimated by the Welch periodogram method using a 1.2 MS data set divided into 8 overlapping sections and is plotted in Fig.7 is corrupted by switching noise as expected. In particular, Fig.7 shows the measured v_c spectra for a non-modulated PWM signal and for a random SS-modulated PWM, with a modulation profile $\xi(t)$ as in (5) where random variables r_k have been obtained sampling thermal noise, with a modulation depth $\delta = 6\%$. It can be observed that the harmonic peaks are reduced from 5 to 15 dB due to SS modulation as expected from previous studies [13]. Moreover, in Fig.8, the measured harmonic peak reduction (markers in Fig.8) is in fair agreement with the rough EMI p.s.d. estimate

$$S_{\mathrm{EMI,SS}}(kf_0) \simeq \frac{P_k}{k\delta f_0} \tag{14}$$

obtained assuming that the same EMI power in the non-SS case is uniformly spread over a bandwith $\delta k f_0$ around each harmonic (continuous line in Fig.8) when applying random SS modulations.

B. TEST RESULTS

To validate the EMI-induced channel capacity loss model introduced in Section III, it is now assumed that the transmitter in Fig.4 generates a nominal data stream described as a band-limited Gaussian random process with a uniform p.s.d. over its bandwidth. The background noise, not related to the DC-DC converter operation and including the noise floor of the test instrument, is described as a white Gaussian noise with a p.s.d. $N_0 = -104$ dBm/Hz and the channel capacity has been evaluated from experimental data by (1), considering the combined effects of EMI and of the background noise.

Under the same assumptions, the channel capacity in the presence of EMI has been evaluated by (13), considering the spectral lines falling within the channel bandwidth, with and without SS modulation.

The channel capacity obtained analytically and based on measurements are compared in Fig.9 for a nominal signal bandwidth of 1 MHz at different nominal signal power level at the receiver ranging from -40 dBm up to 10 dBm. The same comparison is performed in Fig.10 for a constant received signal power -20 dBm and different channel bandwidth ranging from 250 kHz up to 2.5 MHz. In both cases, model predictions are in good agreement with measured results, even when the spreading bandwidths of high-order harmonics overlap, i.e. when the assumption of non-overlapping lines considered in the derivation of (13) is not met.

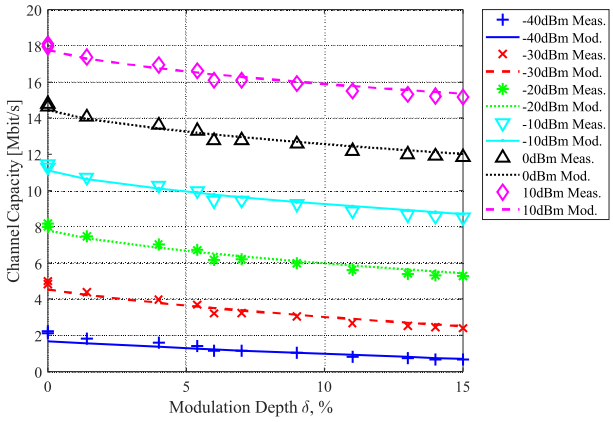

FIGURE 9. Capacity of a 1 MHz communication channel corrupted by SS-modulated EMI vs. modulation depth δ at a different nominal received signal power level (assumed uniformly distributed over the channel bandwidth): measured results versus prediction obtained from (13).

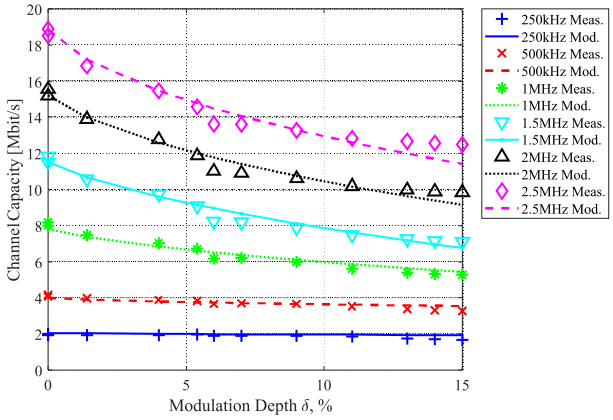

FIGURE 10. Capacity of a communication channel corrupted by SS-modulated EMI vs. modulation depth δ for different channel bandwidth at constant nominal received signal power, assumed uniformly distributed over the channel bandwidth: measured results versus prediction obtained from (13).

V. DISCUSSION

Based on the results presented in Section III and validated in Section IV, a qualitative analysis of the effects of SS modulation on channel capacity is now proposed.

From (11) in Section III, in particular, at a fixed signal-to-background noise ratio α and EMI-to-signal power β, the reduction in channel capacity ΔC depends on the bandwidth W over which the EMI power is spread due to the combined effect of two contrasting mechanisms: the first, related to the multiplying factor $W^\star$, equal to W in case of full inclusion of the EMI bandwidth into the signal bandwidth ($W \subset B$), leads to a linearly increasing capacity loss for increasing W, while the second, related to W/B appearing in the argument of the logarithm, leads to an asymptotic reduction of ΔC at increasing W. The net effect of the two mechanisms leads to a non-straightforward dependence of ΔC on the spreading bandwidth W, which will be analyzed in what follows to discuss the effectiveness of SS techniques in practical cases.

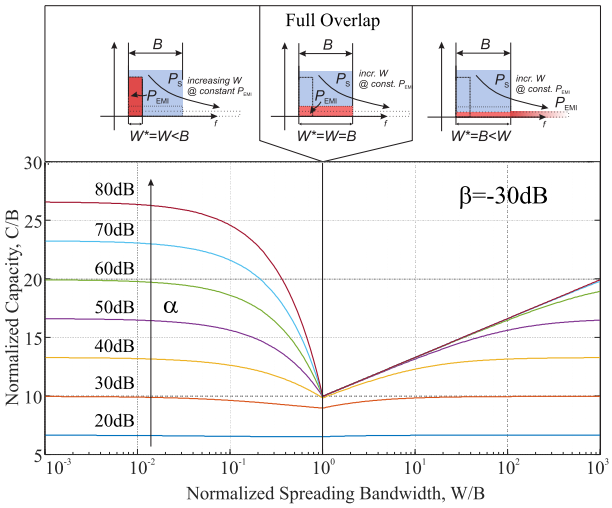

FIGURE 11. Calculated normalized capacity C/B of a communication channel with bandwidth B and constant $P_{EMI}/P_S = -30$ dB, at different signal-to-background noise ratio $\alpha = P_S/(BN_0)$, versus the EMI spreading bandwidth normalized w.r.t. the signal bandwidth W/B.

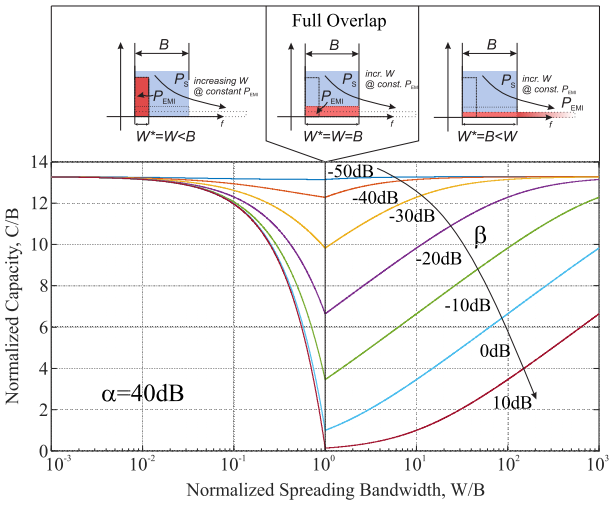

FIGURE 12. Calculated normalized capacity C/B of a communication channel with bandwidth B versus P_{EMI}/P_S ratio, at constant signal-to-background noise ratio $\alpha = 40$dB, versus the EMI spreading bandwidth normalized w.r.t. the signal bandwidth W/B.

For this purpose, the channel capacity due to a single EMI spectral line overlapping the communication channel bandwidth, evaluated as in (11), is plotted in Fig.11 versus the spreading bandwidth W normalized with respect to the victim channel bandwidth B, at different signal-to-background noise ratios α ranging from 20 dB up to 80 dB and for a constant EMI-to-signal power ratio $\beta = P_{\rm EMI}/P_{\rm S} = -30$ dB, assuming that the lower frequency f_0 of the EMI bandwidth coincides with the lower frequency of the signal bandwidth and that the EMI power is uniformly spread upwards from f_0 up to frequency $f_0 + W$. In Fig.12, the capacity is reported for constant signal-to-background noise ratio $\alpha = 40$ dB at different EMI-to-signal power ratios β ranging from -50 dB up to 10 dB.

A. SPREADING BANDWIDTH W FULLY INCLUDED IN THE SIGNAL BANDWIDTH B

In Fig.11 and Fig.12 for $W/B \leq 1$ it can be observed that the channel capacity loss increases for an increasing spreading bandwidth W. In these cases, in fact, the EMI spectral line is fully included in the signal bandwidth and $W^\star = W$. Moreover, assuming that the spread EMI p.s.d. is larger[2] than the background noise p.s.d. N_0 and can be therefore regarded as the capacity limiting factor, i.e. for $P_{\mathrm{EMI}}/W \gg N_0$, it follows that

$$\alpha\beta = \frac{P_{\mathrm{S}}}{BN_0}\frac{P_{\mathrm{EMI}}}{P_{\mathrm{S}}} \gg \frac{W}{B}. \tag{15}$$

Since the last fraction is the argument of the logarithm of the expression of ΔC in (11), it tends to unity independently of W and (11) reduces to:

$$C \simeq C_0 - W\log_2(1+\alpha). \tag{16}$$

Based on (16), the capacity in the presence of EMI decreases linearly with W, reaching a minimum when the EMI power is spread over the whole channel bandwidth ($W/B \leq 1$ in Fig.11 and 12). Under this condition, the capacity is significantly reduced of 30% and 50% compared to its EMI-free value C_0 even for a relatively low EMI-to-signal power ratio β of -30 dB and -20 dB, respectively. It is worth being observed that, at the same EMI-to-signal power ratio, the EMI-induced capacity loss would be almost negligible for $W/B < 1\%$, i.e. in the case of non-spread EMI.

From Fig.11 and Fig.12, for $W/B \leq 1$ the capacity loss due to an increasing spreading bandwidth W is moderate only if the EMI power is below the background noise power ($\alpha < 30\ \mathrm{dB} = -10\log_{10}\beta$ in Fig.11 and $\beta < -40\ \mathrm{dB} = -10\log_{10}\alpha$ in Fig.12) where (15) is no longer verified and in particular for $P_{\mathrm{EMI}}/W \ll N_0$,

$$C \simeq C_0 - B\frac{\alpha\beta}{\log 2}\frac{\alpha}{1+\alpha} = C_0 - \frac{P_{\mathrm{EMI}}}{N_0\log 2}\frac{\alpha}{1+\alpha} \tag{17}$$

independently of W. In this last case, however, the overall channel capacity is limited by the background noise rather than by EMI and is therefore of limited interest when discussing EMI reduction techniques.

B. SPREADING BANDWIDTH W PARTIALLY OVERLAPPED WITH THE SIGNAL BANDWIDTH B

With reference to Fig.11 and Fig.12, it can be observed that for $W/B > 1$, a further increase of W leads to a reduction in the EMI-induced capacity loss ΔC, which can be explained since the overlap bandwidth $W^\star$ remains constant and equal to the whole signal bandwidth B and part of the EMI power P_{EMI} is spread out of the channel bandwidth when further increasing W. Remarkably, this is the case when the signal bandwidth is fully included in the EMI bandwidth, i.e. $B \subset W$. In this case, C_2 in (7) is zero and the overall channel capacity in the presence of EMI is just expressed by (8) and an increased spreading bandwidth W leads to an increased SNR

$$SNR = \frac{1}{\frac{1}{\alpha} + \frac{B}{W}\frac{1}{\beta}} \tag{18}$$

in the channel bandwidth for $W/B < \alpha\beta$, thus effectively mitigating the adverse effects of EMI.

The results discussed so far for $W/B \gg 1$ confirm that spreading EMI power out of the signal bandwidth brings, as expected, to a reduction of its interfering potential, which is actually the intent of SS techniques. The expected improvement in channel capacity, however, is a very weak function of W/B due to the logarithmic dependence highlighted in (8) and a noticeable increase of the signal capacitance requires in practice a spreading bandwidth W of 10x-100x the victim channel bandwidth B, as it appears in Fig.11 and Fig.12, where the W/B axes are in logarithmic scale. By contrast, keeping the EMI bandwidth to less than a few percent of the signal bandwidth would result in an almost negligible loss in the channel capacity, even when EMI power is comparable with signal power. The results derived above will be validated and contextualized in the following section to discuss the effectiveness of SS techniques under real world application scenarios.

VI. EFFECTIVENESS OF SPREAD SPECTRUM MODULATIONS IN DIFFERENT APPLICATION SCENARIOS

In the previous Sections, the EMI-induced impairment in a communication channel has been quantitatively assessed in a completely general, coding-independent way in terms of an equivalent channel capacity loss. Even if it is reasonable to expect that a channel with a higher capacity achieves better performance under the same communication scheme, a direct link between channel capacity and BER in a specific communication system cannot be established. For this reason, the results presented in Section III will be contextualized to discuss the consistency of the proposed analysis in practical application scenarios.

For this purpose, the effects of SS-modulated and non-modulated EMI generated from a digital equipment interfering with analog narrowband communications, as in [33], will be first considered. Then, the interfering potential of SS-modulated and non-modulated interference generated by DC-DC power converters on baseband digital communications, as in [37], will be focused. Finally, in the last scenario, the case of a digital link with turbo coding, which makes it possible to achieve a data rate approaching the channel capacity and where the effects of EMI-induced capacity loss can be expected to be more evident, is analyzed.

A. NARROWBAND ANALOG COMMUNICATIONS

When considering the interference of a digital device with narrowband analog communications, like the frequency-modulated (FM) radio channel, as considered in [33], EMI

[2]This is the case, in particular, when the EMI power is larger than the overall background noise power integrated in the signal bandwidth since, for $W/B < 1$, $P_{\mathrm{EMI}} > N_0\,B$ implies $P_{\mathrm{EMI}}/W > P_{\mathrm{EMI}}/B > N_0$.

is mostly related with clock waveforms. Such interfering signals have a fundamental frequency f_0 ranging from 10 MHz up to 1 GHz or more which, depending on the coupling $G(f)$ in Fig.1, may show relevant energy at harmonic frequencies kf_0 in the whole 10 MHz-10 GHz frequency range, and are likely to fully overlap with narrowband (<9 kHz) analog FM radio channels even without applying SS modulations. As a consequence, the results considered in Section IVb apply to this case and an increase both in the capacity and in the SNR of the channel is achieved by SS modulation which spread EMI energy out of the signal bandwidth.

In this case, the functionality of the victim FM radio receiver can be preserved thanks to SS, as practically shown in [33], which is therefore consistent with our analysis. These results suggest that SS modulations can be effectively employed in clock generators to avoid received signal quality degradation in analog radio receivers located nearby.[3]

The same conclusions also apply to digital communications whenever a critical information (e.g. timing information) is associated to the spectral content of the transmitted signal in correspondence to the switching frequency of the power converter and, as a result, even in this case the SS is expected to have a beneficial effect.

B. BASEBAND DIGITAL COMMUNICATIONS

When the interference of switching-mode power converters with baseband digital communication lines is considered, EMI from the power converters has a fundamental frequency ranging from 10 kHz to 1 MHz and shows relevant energy content only below 10 MHz, potentially interfering with digital baseband communication channels, whose bandwidth ranges in the 10 kHz-10 MHz range. In such a situation, the channel bandwidth easily overlaps with several EMI harmonics, both in case of periodic and SS-modulated EMI. As a consequence, for each spectral line, the considerations presented in Section IVa apply to this scenario, and a channel capacity reduction is expected when SS modulation is applied.

Such a reduction, however, is not necessarily translated into an increased BER, since the data rate achievable by practical communication schemes could be significantly lower than the Shannon capacity limit and a direct relation between channel capacity and BER cannot be generally established.

As a matter of fact, when transmitting digital information without specific coding on a channel corrupted by EMI, as in [37], the BER appears to be not affected by SS modulations, as shown in the experimental results presented in [37] and also reported in Fig.13 for convenience, where the measured BER of an I^2C link [39] coupled with periodic and SS-modulated EMI from the same DC-DC converter are plotted versus the SS modulation depth δ for random and other SS profiles. The results presented in Section IVa and in [37], suggest to circuit designers that, in case of critical interference

[3]This is the typical interference scenario which has been actually considered in the formulation of standard EMC regulations.

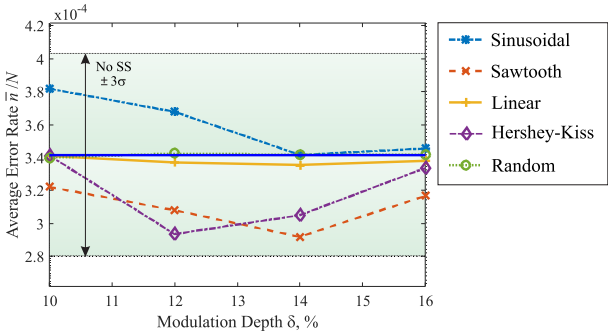

FIGURE 13. Measurement results: average error rate $\bar{n}/N$ versus the modulation depth δ for different modulation profiles [37].

of power systems and simple data links commonly employed at PCB and IC level, no substantial enhancement can be expected by adopting SS techniques.

C. TURBO-CODED DIGITAL COMMUNICATIONS

Based on the same argument considered above, it is reasonable to expect that the EMI-induced channel capacity reduction can be more directly linked to BER performance degradation at data rates approaching the Shannon limit, which can be achieved in practice using appropriate channel coding [40], [41]. This consideration suggests a worse impact of SS-modulated EMI compared to non-modulated EMI with the same power in communication systems featuring advanced channel coding techniques (e.g. turbo coding).

To investigate this hypothesis, a two-level phase shift keying (2-PSK) digital link over an AWGN channel with $B = 600$ kHz bandwidth, corrupted by non-modulated and SS-modulated EMI measured with the test setup in Fig.4, has been simulated in the Matlab environment. In this simulation, symbols are assumed to be transmitted over the channel at 500 kbaud, corresponding to a net bit rate of 166 kbps in view of the $R = 1/3$ rate of the Turbo code. A signal-to-background noise ratio $E_b/N_0 = 4.8$ dB is considered. The performance in terms of BER of data transmission employing a Turbo code has been compared for different EMI amplitude and applying random SS-modulations with different depth δ. More details about the Turbo code are reported in the Appendix.

In Fig.14, in particular, the BER is plotted versus the r.m.s. EMI amplitude (disturbances with different amplitudes have been obtained applying a scaling factor to the same measured EMI waveforms) for different values of δ. From the figure, it can be observed that the EMI amplitude at which BER starts increasing in a significant way is lower for a larger SS-modulation depth and higher in the non-modulated case or for smaller values of δ. In particular, comparing non-modulated EMI with SS-modulated EMI, a similar BER is achieved for a 15% higher EMI amplitude in the non-modulated cases, which is consistent with the EMI-induced capacity loss vs. SS-modulation depth analysis presented in

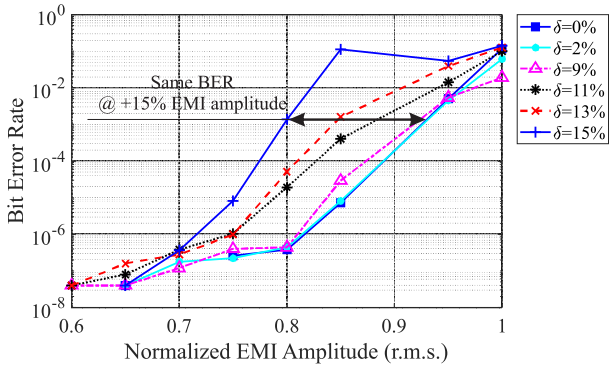

FIGURE 14. Bit error rate of a communication channel corrupted by SS-modulated EMI vs. EMI normalized r.m.s. amplitude at different modulation depth δ.

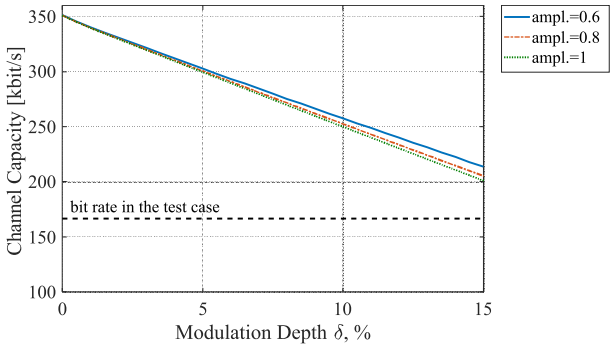

FIGURE 15. Capacity of the channel considered in the Turbo-coded communication evaluated by (13) versus modulation depth δ at different EMI normalized amplitude.

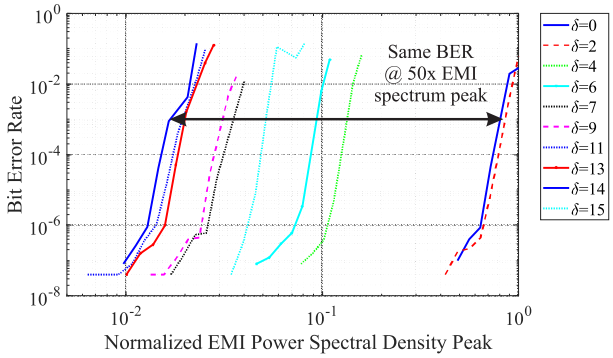

FIGURE 16. Bit error rate of a communication channel corrupted by SS-modulated EMI vs. EMI power spectral density peak (normalized w.r.t. its maximum value without SS modulation) at different modulation depth δ.

this paper and contextualized for the above test conditions in Fig.15.

The worse adverse impact of SS-modulated EMI is even more evident in Fig.16, where the BER is plotted versus the normalized p.s.d. peak value of the EMI spectrum in the communication channel bandwidth normally taken into account for EMI compliance [9], [10], under the same test conditions of Fig.14. The plot reveals that the same 10^{-3} BER achieved at $\delta = 14\%$ SS-modulation depth can be obtained

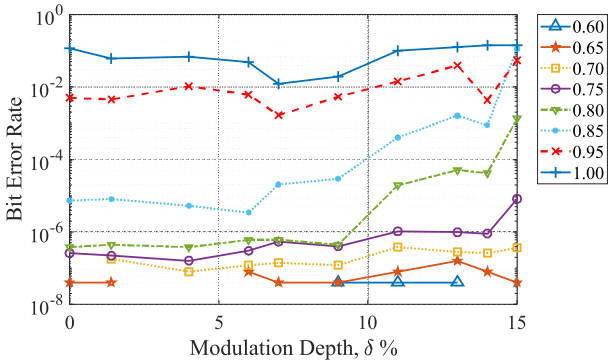

FIGURE 17. Bit error rate of a communication channel corrupted by SS-modulated EMI vs. different modulation depth δ at different EMI normalized r.m.s. amplitude values.

for a non-modulated EMI with a 50X higher EMI spectrum peak.

With reference to the same communication channel, the BER is also plotted in Fig.17 versus the modulation depth δ for different EMI amplitude. The results reported in the figure confirm a consistent increasing trend of the BER at a fixed EMI amplitude and show that above 5%-6% modulation depth, a nonzero BER is observed also at EMI amplitude for which no errors have been reported for the non-modulated case. These results warn designers about possible detrimental effects of SS modulations when the interference of power converters and advanced communication systems is considered.

VII. CONCLUSION

The effects of EMI on a communication channel have been described in terms of an equivalent channel capacity loss so that to analyze and compare the effects of non-modulated and random SS-modulated EMI at different modulation depths. The EMI-induced capacity loss has been analytically predicted and found in good agreement with experiments. In this framework, the EMI-induced capacity loss due to non-modulated and SS-modulated EMI has been studied in practical application scenarios and its relation with measured/simulated BER is discussed, revealing that SS-modulated EMI can show a worse interfering potential compared to non-modulated EMI in a digital link featuring advanced channel coding to approach the Shannon capacity limit.

These results are valuable to electronic system designers who consider the adoption of SS in their products. From a different perspective, the same results point out a limitation of standard EMC measurement methods, which just consider the peaks of EMI spectra as a benchmark. According to such standard EMC test methods, in fact, the application of SS modulations always results in an improvement and the worse detrimental effect of SS-EMI in terms of EMI-induced capacity loss is not highlighted.

Application of the proposed method to real-world communication channels will be considered in future works.

APPENDIX

The BER performance of a communication using Turbo codes over an AWGN corrupted by EMI presented in Section V.c has been simulated using the Matlab Communication Toolbox, adapting the procedure described in [42], p.4-13, using randomly generated binary data arranged in frames of 4096 bits, turbo-encoding the data using random interleaver indices. Encoded data are transmitted by a 2-PSK modulation over the AWGN channel corrupted by EMI as described in the text and then demodulated. The log-likelihood ratio (LLR) of the received stream is then evaluated in order to output soft bits to the Turbo decoder, whose number of iterations is set to four. The error statics are finally calculated.

REFERENCES

[1] S. Ben Dhia, M. Ramdani, and E. Sicard, *Electromagnetic Compatibility of Integrated Circuits: Techniques for Low Emission and Susceptibility*. New York, NY, USA: Springer, 2006.

[2] F. Musolino, Y. Villavicencio, and F. Fiori, "Chip-level design constraints to comply with conducted electromagnetic emission specifications," *IEEE Trans. Electromagn. Compat.*, vol. 54, no. 5, pp. 1137–1146, Oct. 2012.

[3] P. S. Crovetti and F. L. Fiori, "Efficient BEM-based substrate network extraction in silicon SoCs," *Microelectron. J.*, vol. 39, pp. 1774–1784, Dec. 2008.

[4] P. S. Crovetti and F. Fiori, "Distributed conversion of common-mode into differential-mode interference," *IEEE Trans. Microw. Theory Techn.*, vol. 59, no. 8, pp. 2140–2150, Aug. 2011.

[5] P. S. Crovetti and F. L. Fiori, "A linear voltage regulator model for EMC analysis," *IEEE Trans. Power Electron.*, vol. 22, no. 6, pp. 2282–2292, Nov. 2007.

[6] Y. Matsumoto, T. Shimizu, T. Murakami, K. Fujii, and A. Sugiura, "Impact of frequency-modulated harmonic noises from pcs on OFDM-based WLAN systems," *IEEE Trans. Electromagn. Compat.*, vol. 49, no. 2, pp. 455–462, May 2007.

[7] *Code of Federal Regulations, Title 47, Chapter I, Subchapter A, Part 15, Subpart B: Unintentional Radiators*. Accessed: Jul. 19, 2018. [Online]. Available: https://www.ecfr.gov/

[8] "Council directive 89/336/EEC of 3 May 1989 on the approximation of the laws of the member states relating to electromagnetic compatibility," Offcial J. Council Eur. Union, Bruxelles, Belgium, Tech. Rep. L139/19, May 1989.

[9] *Industrial, Scientific and Medical Equipment—Radio-Frequency Disturbance Characteristics—Limits and Methods of Measurement*, Standard CISPR 11:2015, IEC, 2015.

[10] *Electromagnetic Compatibility—Requirements for Household Appliances, Electric Tools and Similar Apparatus—Part 1: Emission*, Standard CISPR 14-1:2016, IEC, 2016.

[11] Y. Lobsiger and J. W. Kolar, "Closed-loop di/dt and dv/dt IGBT gate drive concepts," *IEEE Trans. Power Electron.*, vol. 30, no. 6, pp. 3402–3417, Jun. 2015.

[12] H. Chung, S. Y. R. Hui, and K. K. Tse, "Reduction of power converter EMI emission using soft-switching technique," *IEEE Trans. Electromagn. Compat.*, vol. 40, no. 3, pp. 282–287, Aug. 1998.

[13] F. Pareschi, R. Rovatti, and G. Setti, "EMI reduction via spread spectrum in DC/DC converters: State of the art, optimization, and tradeoffs," *IEEE Access*, vol. 3, pp. 2857–2874, 2015.

[14] F. Musolino and F. Fiori, "Investigations on the Susceptibility of ICs to Power-Switching Transients," *IEEE Trans. Power Electron.*, vol. 25, no. 1, pp. 142–151, Jan. 2010.

[15] F. Lin and D. Y. Chen, "Reduction of power supply EMI emission by switching frequency modulation," *IEEE Trans. Power Electron.*, vol. 9, no. 1, pp. 132–137, Jan. 1994.

[16] K. B. Hardin, J. T. Fessler, and D. R. Bush, "Spread spectrum clock generation for the reduction of radiated emissions," in *Proc. IEEE Symp. Electromagn. Compat.*, Chicago, IL, USA, Aug. 1994, pp. 227–231.

[17] S. Callegari, R. Rovatti, and G. Setti, "Spectral properties of chaos-based FM signals: Theory and simulation results," *IEEE Trans. Circuits Syst. I, Fundam. Theory Appl.*, vol. 50, no. 1, pp. 3–15, Jan. 2003.

[18] G. Setti, M. Balestra, and R. Rovatti, "Experimental verification of enhanced electromagnetic compatibility in chaotic FM clock signals," in *Proc. IEEE Int. Symp. Circuits Syst.*, vol. 3. May 2000, pp. 229–232.

[19] K. K. Tse, H. S.-H. Chung, S. Y. R. Hui, and H. C. So, "A comparative study of carrier-frequency modulation techniques for conducted EMI suppression in PWM converters," *IEEE Trans. Ind. Electron.*, vol. 49, no. 3, pp. 618–627, Jun. 2002.

[20] F. Pareschi, G. Setti, R. Rovatti, and G. Frattini, "Short-term optimized spread spectrum clock generator for EMI reduction in switching DC/DC converters," *IEEE Trans. Circuits Syst. I, Reg. Papers*, vol. 61, no. 10, pp. 3044–3053, Oct. 2014.

[21] A. Bendicks, S. Frei, N. Hees, and M. Wiegand, "Systematic reduction of peak and average emissions of power electronic converters by the application of spread spectrum," *IEEE Trans. Electromagn. Compat.*, vol. 60, no. 5, pp. 1571–1580, Oct. 2018.

[22] K. Cui, V. Adrian, B.-H. Gwee, and J. S. Chang, "A noise-shaped randomized modulation for switched-mode DC-DC converters," *IEEE Trans. Circuits Syst. I, Reg. Papers*, vol. 65, no. 1, pp. 394–405, Jan. 2018.

[23] E. N. Y. Ho and P. K. T. Mok, "Design of PWM ramp signal in voltage-mode CCM random switching frequency buck converter for conductive emi reduction," *IEEE Trans. Circuits Syst. I, Reg. Papers*, vol. 60, no. 2, pp. 505–515, Feb. 2013.

[24] A. Santolaria, "Effects of switching frequency modulation on the power converter's output voltage," *IEEE Trans. Ind. Electron.*, vol. 56, no. 7, pp. 2729–2737, Jul. 2009.

[25] D. Gonzalez, J. Balcells, A. Santolaria, J.-C. Le Bunetel, J. Gago, D. Magnon, and S. Brehaut, "Conducted EMI reduction in power converters by means of periodic switching frequency modulation," *IEEE Trans. Power Electron.*, vol. 22, no. 6, pp. 2271–2281, Nov. 2007.

[26] J. Lapiedra, "Spread spectrum clocking using the CDCS502/503," Texas Instrum., Dallas, TX, USA, Appl. Note SCAA103, Aug. 2009.

[27] "STM32 MCUs spread-spectrum clock generation principles, properties and implementation," STMicroelectronics, Geneva, Switzerland, Appl. Note AN4850, Jul. 2016.

[28] *R1275S Series, 30V, 2A, Synchronous PWM Step-down DC/DC Converter*, Ricoh Electron. Devices. [Online]. Available: https://www.e-devices.ricoh.co.jp/en/products/power/dcdc/r1275/r1275-ea.pdf

[29] *Multiphase Oscillator With Spread Spectrum Frequency Modulation*, document LTC6902, Linear Technology, Milpitas, CA, USA, 2003. [Online]. Available: http://cds.linear.com/docs/en/datasheet/6902f.pdf

[30] D. Lauder, and J. Moritz, "Investigation into possible effects resulting from dithered clock oscillators on EMC measurements and interference to radio transmission systems," Radiocommun. Agency, London, U.K., Tech. Rep. REF AY3377, 2000.

[31] K. Hardin, R. A. Oglesbee, and F. Fisher, "Investigation into the interference potential of spread-spectrum clock generation to broadband digital communications," *IEEE Trans. Electromagn. Compat.*, vol. 45, no. 1, pp. 10–21, Feb. 2003.

[32] R. Mukherjee, A. Patra, and S. Banerjee, "Impact of a frequency modulated pulsewidth modulation (PWM) switching converter on the input power system quality," *IEEE Trans. Power Electron.*, vol. 25, no. 6, pp. 1450–1459, Jun. 2010.

[33] H. G. Skinner and K. P. Slattery, "Why spread spectrum clocking of computing devices is not cheating," in *Proc. IEEE EMC Int. Symp., Symp. Rec., Int. Symp. Electromagn. Compat.*, Aug. 2001, pp. 537–540.

[34] C. E. Shannon, "A mathematical theory of communication," *Bell Syst. Tech. J.*, vol. 27, p. 379, 1948.

[35] H. Meng, Y. L. Guan, and S. Chen, "Modeling and analysis of noise effects on broadband power-line communications," *IEEE Trans. Power Del.*, vol. 20, no. 2, pp. 630–637, Apr. 2005.

[36] T. M. Cover and J. A. Thomas, *Elements of Information Theory* (Telecommunications and Signal Processing), 2nd ed. New York, NY, USA: Wiley, 2006.

[37] F. Musolino and P. S. Crovetti, "Interference of spread-spectrum switching-mode power converters and low-frequency digital lines," in *Proc. IEEE Int. Symp. Circuits Syst. (ISCAS)*, Florence, Italy, May 2018, pp. 1–5.

[38] C. R. Paul, *Introduction to Electromagnetic Compatibility*. New York, NY, USA: Wiley, 2006.

[39] *I2C-Bus Specification User Manual*, NXP Semicondutors, Eindhoven, The Netherlands, Apr. 2014.

[40] C. Berrou, A. Glavieux, and P. Thitimajshima, "Near Shannon limit error-correcting coding and decoding: Turbo-codes. 1," in *Proc. IEEE Int. Conf. Commu.*, Geneva, Switzerland, May 1993, pp. 1064–1070.

[41] S. Benedetto, G. Montorsi, D. Divsalar, and F. Pollara, "A soft-input soft-output maximum a posteriori (MAP) module to decode parallel and serial concatenated codes," *Jet Propuls. Lab TDA Progr. Rep.*, vol. 42, p. 127, Nov. 1996.
[42] MathWorks. (Nov. 2018). *Communications Toolbox: User's Guide (R2018b)*. [Online]. Available: https://it.mathworks.com/help/pdf_doc/comm/comm.pdf

FRANCESCO MUSOLINO (S'01–M'03) was born in Torino, Italy, in 1972. He received the Laurea and Ph.D. degrees in electronic engineering from the Politecnico di Torino, Torino, Italy, in 1999 and 2003, respectively. He is currently a Researcher with the Department of Electronics and Telecommunications (DET), Politecnico di Torino, where he teaches courses on fundamental electronics and electronics for electric drives. His research interests include electronics for power conversion and motor drive applications, mixed-signal circuits, electromagnetic compatibility at the system levels and the analysis, modeling, and experimental characterization of electromagnetic compatibility problems at the printed circuit board and package level.

PAOLO S. CROVETTI (S'00–M'04) was born in Turin, Italy, in 1976. He received the Laurea *(summa cum laude)* and Ph.D. degrees in electronic engineering from the Politecnico di Turin, Turin, Italy, in 2000 and 2003, respectively. He is currently an Associate Professor with the Department of Electronics and Telecommunications (DET), Politecnico di Torino, Turin, where he teaches courses on fundamental and automotive electronics. He has coauthored more than 50 articles appearing in journals and international conference proceedings. His main research interests include analog, mixed-signal and power integrated circuits, and electromagnetic compatibility. His recent research activities are focused on non-conventional information and power processing techniques, and ultra-low-power IC design for the Internet of Things. He was a Corecipient of the Excellent Paper Award from the EMC 2009 Kyoto Symposium, in 2009. He is an Associate Editor of the IEEE TRANSACTIONS ON VLSI SYSTEMS and a Subject Editor of *IET Electronics Letters* in the areas of circuits and systems. He also serves as a regular Reviewer for several IEEE journals.